Drug Design, Development and Therapy

Dovepress
Taylor & Francis Group

Open Access Full Text Article

ORIGINAL RESEARCH

Vitamin K_2 Protects Against Glucocorticoid-Induced Osteoporosis by Activating the NRF2/FSP1 Pathway to Inhibit Osteoblast Ferroptosis

Zhichao Zhang[1–4], Xing Rong[1,3], Qinghua Ren[1,3], Yuying Kou[5], Jie Guo[1–3], Minqi Li[1,3]

[1]Department of Bone Metabolism, School and Hospital of Stomatology, Cheeloo College of Medicine, Shandong University & Shandong Key Laboratory of Oral Tissue Regeneration & Shandong Engineering Research Center of Dental Materials and Oral Tissue Regeneration & Shandong Provincial Clinical Research Center for Oral Diseases, Jinan, Shandong, People's Republic of China; [2]Department of Orthodontics, School and Hospital of Stomatology, Cheeloo College of Medicine, Shandong University, Jinan, Shandong, People's Republic of China; [3]Center of Osteoporosis and Bone Mineral Research, Shandong University, Jinan, Shandong, People's Republic of China; [4]Department of Stomatology, The Second Hospital of Shandong University, Jinan, Shandong, People's Republic of China; [5]School of Stomatology, Shandong First Medical University & Shandong Academy of Medical Sciences, Jinan, Shandong, People's Republic of China

Correspondence: Jie Guo, Department of Orthodontics, School and Hospital of Stomatology, Cheeloo College of Medicine, Shandong University, No. 44-1 Wenhua Road West, Jinan, Shandong, 250012, People's Republic of China, Fax +8653188382923, Email kqgj@sdu.edu.cn; Yuying Kou, School of Stomatology, Shandong First Medical University & Shandong Academy of Medical Sciences, No. 6699 Qingdao Road, Jinan, Shandong, 250117, People's Republic of China, Fax +8653159556822, Email 1453870058@qq.com

Purpose: Glucocorticoid-induced osteoporosis (GIOP) is the most common form of secondary osteoporosis, and its pathogenesis is closely associated with oxidative stress and impaired osteogenic differentiation. Vitamin K_2 (VK_2) has strong antioxidant properties and potent bone-forming effects, but its application in GIOP is still unclear. This study investigates the therapeutic potential of VK_2 in GIOP and elucidates its underlying molecular mechanisms.

Methods: Dexamethasone (DEX) was used to establish GIOP model within C57BL/6 mice. The bone mass was assessed using micro-computed tomography (micro-CT), hematoxylin and eosin (HE) staining, and Masson's trichrome staining in vivo. The osteoblast activity and the expression of osteogenic and ferroptosis-related markers were evaluated via immunohistochemistry (IHC), RT-qPCR, Western blotting, ALP and alizarin red staining. The mitochondrial function and lipid peroxidation of MC3T3-E1 cells were detected by flow cytometry, immunofluorescence and specific kits.

Results: VK_2 partially prevented bone mass reduction and osteoblast activity inhibition in GIOP mice. VK_2 not only reversed the DEX-induced reductions in Tb.N, BV/TV, and Tb.Th, but also significantly increased the expression of osteogenic markers, including OCN and ALP ($P<0.05$). Moreover, VK_2 improved DEX-induced ferroptosis, oxidative stress and mitochondrial dysfunction in MC3T3-E1 cells and promoted osteogenic differentiation in vitro, which could be reversed by ferroptosis inducer ($P<0.05$). VK_2 also increased the expression of NRF2, HO-1 and FSP1 which inhibited by DEX in vivo and in vitro ($P<0.05$). The inhibition of FSP1 and NRF2 reversed the osteogenic differentiation promotion and ferroptosis inhibition by VK_2 ($P<0.05$).

Conclusion: VK_2 restores mitochondrial function and reduces lipid peroxidation and ferroptosis via the NRF2/FSP1 signaling pathway, thereby facilitating osteoblast differentiation and improving bone mass in GIOP mice. This finding not only provides a fresh perspective on the etiology of GIOP but also positions ferroptosis inhibition as a promising and innovative therapeutic strategy for this condition, with VK_2 emerging as a potential candidate for clinical translation.

Keywords: GIOP, VK_2, osteoblast, ferroptosis, NRF2, FSP1

Introduction

Glucocorticoids (GCs) are commonly employed to alleviate inflammation or inhibit the immune system.[1,2] It has been reported that long-term glucocorticoid prescriptions have increased by more than 30% over the past two decades.[3]

Received: 11 August 2025
Accepted: 17 December 2025
Published: 23 December 2025

Among the adverse effects associated with glucocorticoid therapy, GIOP represents the most prevalent form of iatrogenic and secondary osteoporosis. The pathophysiological mechanism of GIOP is highly complex, characterized by a sustained reduction in bone formation and a transient early increase in bone resorption.[2] Consequently, promoting bone formation has become a crucial therapeutic objective in GIOP, a condition marked by considerable limitations in current management options. Anti-resorptive agents (eg, bisphosphonates) effectively suppress bone resorption; however, a significant limitation is that they do not address the underlying cause of impaired bone formation. Furthermore, their long-term use is associated with severe complications such as osteomyelitis and osteonecrosis.[4,5] Anabolic therapies such as teriparatide can stimulate bone formation, but their clinical utility is limited by high costs, cumbersome administration, and significant safety concerns, including hypercalcemia and an elevated risk of infection.[6,7] The further elucidation of the underlying pathogenic mechanisms and the identification of safer and more effective pharmacological agents remain urgent challenges in clinical practice.

VK_2 is primarily derived from fermented foods and is considered to have a favorable safety profile profile.[8,9] The biological activity of VK_2 is attributed to its unique molecular structure and potent antioxidant properties. As a fat-soluble vitamin, VK_2 readily permeates cell membranes and enters intracellular compartments to exert its protective effects.[10] VK_2 has been reported to restore metabolic balance in bone tissue and to regulate bone remodeling bidirectionally by promoting bone formation and inhibiting bone resorption.[11] Distinguished from other osteoporosis therapeutics, VK_2 emerges as a promising alternative by uniquely targeting impaired bone formation through dual anabolic and cytoprotective mechanisms. Its capacity to enhance osteogenic function, coupled with oral bioavailability, a favorable safety profile, and cost-effectiveness, positions VK_2 as a viable long-term strategy that addresses critical gaps in current GIOP management. In recent years, multiple studies have demonstrated that VK_2 exhibits significant therapeutic effects in treating primary osteoporosis and diabetic osteoporosis, particularly in maintaining and improving bone density and reducing the incidence of fractures.[12,13] Clinical studies also provide a compelling body of evidence supporting the skeletal benefits of VK_2 in postmenopausal women. Knapen demonstrated that VK_2 supplementation significantly enhances bone mineral content and femoral neck width,[14] while Koitaya reported that even low-dose VK_2 improves bone metabolism biomarkers and inhibits bone loss.[15] Most importantly, these benefits translate into a definitive clinical outcome: multiple prospective intervention trials have consistently shown that VK_2 supplementation reduces the risk of vertebral fractures by approximately 60% in this population.[16–18] These consistent findings strongly advocate for the use of VK_2 in osteoporosis prevention and management. Our previous research also demonstrated that VK_2 significantly mitigated the progression of osteonecrosis of the jaw by promoting osteoblast differentiation.[19] Despite emerging evidence, the precise role and underlying molecular mechanisms of VK_2 in GIOP remain poorly understood and warrant further investigation.

Ferroptosis is a novel form of programmed cell death characterized by the iron-dependent accumulation of reactive oxygen species (ROS), which catalyzing the peroxidation of polyunsaturated fatty acids in cellular membranes, ultimately resulting in membrane disruption and cell death.[20–22] FSP1 (formerly AIFM2) is a crucial regulator of ferroptosis that acts independently of GPX4. It catalyzes the NAD(P)H-dependent reduction of COQ10 to its antioxidant form, ubiquinol, which scavenges lipid peroxyl radicals and protects cellular membranes from oxidative damage.[23,24] Emerging evidence has implicated ferroptosis in the pathogenesis of osteoporosis across various etiologies. For instance, VK_2 has been reported to ameliorate type 2 diabetic osteoporosis (DOP) by activating the AMPK/SIRT1 pathway, thereby inhibiting ferroptosis.[25] In a similar context, maresin1 was shown to suppress high-glucose-induced ferroptosis in osteoblasts via NRF2 activation.[26] Furthermore, therapeutic strategies targeting ferroptosis or its associated mediator HO-1 have demonstrated efficacy in rescuing osteocyte death in DOP.[27] This approach works by disrupting the vicious cycle between lipid peroxidation and heme oxygenase-1 (HO-1) activation, ultimately preventing trabecular bone deterioration. Notably, GIOP is often associated with mitochondrial dysfunction and elevated ROS levels, suggesting a potential role of ferroptosis in its development.[28] However, the interplay between VK_2, ferroptosis, and osteoblast function in GIOP remains inadequately explored and poorly understood.

Nuclear factor erythroid 2-related factor 2 (NRF2) is a central transcriptional regulator of the cellular antioxidant defense system, while ferroptosis is a form of regulated cell death driven by iron-dependent lipid peroxidation.[29] NRF2 modulates ferroptosis susceptibility both directly and indirectly by controlling the expression of multiple antioxidants and

cytoprotective genes, such as HO-1, glutathione (GSH), and GPX4.[29–31] Previous studies have demonstrated that FSP1 is a transcriptional target of NRF2, and that the ubiquinone CoQ-FSP1 axis mediates ferroptosis and confers radiation resistance in KEAP1-deficient lung cancer cells.[32] However, the role of this pathway in GIOP remains unexplored. Therefore, it is essential to investigate the potential of VK_2 to alleviate GIOP by modulating ferroptosis in osteoblasts and to elucidate the role of the NRF2/FSP1 signaling axis in the pathogenesis and treatment of this condition.

Therefore, this study aimed to investigate the hypothesis VK_2 protects against GIOP by inhibiting osteoblast ferroptosis through activation of the NRF2/FSP1 signaling pathway. Using a combination of in vivo GIOP mouse models and in vitro systems, we sought to determine whether this mechanism underlies VK_2's efficacy in preventing bone loss and promoting osteogenic differentiation.

Materials and Methods

Establishment of the GIOP Model and Tissue Collection

Thirty 8-week-old male C57BL/6 mice were procured from Jinan Pengyue Experimental Animal Breeding Co., Ltd. (Shandong, China). All animal experiments were approved by the Institutional Animal Care and Use Committee (IACUC), School and Hospital of Stomatology, Shandong University (No.20230803). All treatment procedures were conducted in accordance with the Guidelines for the Care and Use of Laboratory Animals of the National Institutes of Health. Using a random number table mice were randomly allocated to three groups: the control group, the DEX, and the DEX+VK_2 group, with 10 mice in each group. Mice in the DEX and DEX+VK_2 groups were intraperitoneally injected with DEX (DEX; 1 mg/kg, MCE, China) every other day for 8 weeks.[33] Additionally, the DEX+VK_2 group was orally supplemented with VK_2 (VK_2; 30 mg/kg; Glakay, Shibakawa Plant of Fuji Capsule Co., Ltd., Japan) five days per week.[19] After 8 weeks of treatment, all mice were anesthetized and intracardially perfused, and femurs were isolated and collected. Following fixation with 4% paraformaldehyde, the femurs were either used for Micro-CT imaging or subjected to decalcification, dehydration, and paraffin embedding for histological sectioning.

Micro-CT Assessment of the Femurs

Microarchitectural parameters of the collected femurs from all three groups were assessed using a Micro-CT scanner (SCANCO Medical AG, Bruttisellen, Switzerland). Micro-CT images were reconstructed at a resolution of 10 μm (SCANCO Medical AG).

HE Staining and Masson Trichrome

After immersed in xylene for dewaxing and hydrated in descending gradient alcohol, the paraffin sections were stained with hematoxylin followed by eosin (HE staining). Other sections were sequentially stained with hematoxylin and Ponceau S acid fuchsin, rinsed in aqueous glacial acetic acid, differentiated in phosphomolybdic acid solution, and finally immersed in aniline blue solution. After mounting with neutral balsam, the sections were examined under a light microscope (Olympus BX-53, Tokyo, Japan).

IHC Staining

Following dewaxing, hydration, and antigen retrieval, antigenic epitopes were exposed. Endogenous peroxidase activity was inhibited using 0.3% hydrogen peroxide solution, and non-specific binding sites were blocked with 1% bovine serum albumin (BSA) in PBS. Sections were incubated overnight at 4°C with specific primary antibodies, including anti-ALP (ab108337, Abcam), anti-OCN (ab93876, Abcam), anti-FSP1 (20,886-1-AP, Proteintech), anti-NRF2 (T55136, Abmart), and anti-HO-1 (T55113, Abmart), followed by incubation with appropriate secondary antibodies for 1 hour at room temperature. Subsequently, a DAB chromogenic reaction was performed, and sections were counterstained with methyl green. Images were acquired via light microscopy and analyzed using Image Pro Plus 6.0.

Cell Culture and Treatment

The MC3T3-E1 cell line was obtained from the Shanghai Cell Centre (Shanghai, China) and cultured in α-MEM supplemented with 10% fetal bovine serum (FBS), 100 U/mL penicillin, and 100 μg/mL streptomycin in a humidified incubator at 37°C with 5% CO_2. To assess osteogenic capacity, cells in each group were treated with osteogenic induction medium for 7, 14, or 21 days, depending on the experimental design. The osteogenic induction medium consisted of 0.1 μM DEX, 10 mM β-glycerophosphate, and 0.05 mM ascorbic acid. Based on specific experimental objectives, cells were additionally treated with the ferroptosis inducer FIN56 (5μm, HY-103087, MCE, China), the FSP1 inhibitor iFSP1 (3μm, HY-136057, MCE, China), or the NRF2 inhibitor ML385 (50μm, HY-100523, MCE, China), RSL3 (800nM, HY-100218A, MCE, China).

Reverse Transcriptase-Quantitative Polymerase Chain Reaction (qPCR)

Total RNA from MC3T3-E1 cells was extracted using TRIzol reagent (AG21102, Precision Biotechnology) and RNAex Pro Reagent (Accurate Biology, Changsha, China). Reverse transcription to cDNA was performed using the Evo M-MLV Reverse Transcription Kit (Accurate Biology). Quantitative real-time PCR (RT-qPCR) was conducted in quintuplicate using SYBR Green PCR kits (Accurate Biology) on a real-time PCR system (Bio-Rad, Hercules, USA). Relative gene expression levels of ALP, OCN, RUNX2, FSP1, GPX4, SLC7A11, and NRF2 were calculated using the $2^{\wedge-\Delta\Delta Ct}$ method, with GAPDH as the internal reference. All primer sequences are listed in Table 1.

Western Blotting (WB)

Total intracellular proteins were extracted using a mixture of RIPA lysis buffer, protease inhibitor, and phosphatase inhibitor (98:1:1, Cwbio, Beijing, China). Protein concentrations were determined using a BCA protein assay kit (P0012S, Beyotime). Equal amounts of protein (30 μg per lane) were separated by 10% SDS-PAGE and transferred to polyvinylidene fluoride (PVDF) membranes. Membranes were blocked with 5% BSA in TBST for 1 hour at room temperature, followed by overnight incubation at 4°C with the following primary antibodies: anti-ALP (ab108337, Abcam), anti-RUNX2 (ab192256, Abcam), anti-OCN (ab93876, Abcam), anti-GAPDH (ab9485, Abcam), anti-KEAP1 (WL03285, Wanleibio), anti-NRF2 (T55136, Abmart), anti-HO-1 (T55113, Abmart), and anti-FSP1 (20,886-1-AP, Proteintech). After three washes, membranes were incubated for 1 hour at room temperature with horseradish peroxidase (HRP)-conjugated goat anti-rabbit IgG (ab6721, Abcam) or goat anti-mouse IgG (SA00001-1, Proteintech). Protein bands were visualized using a gel imaging system (Amersham Imager 600, General Electric) and quantified with Image-Pro Plus 6.0 (Media Cybernetics), with expression levels normalized to GAPDH.

Table 1 Primer Sequences Used in the Experiment

Gene	Forward	Reverse
ALP	5′-GCGACCACTTGAGCAAACATC-3′	5′-CGGCTGATTGGCTTCTTCTT-3′
OCN	5′-CAGAACAGACAAGTCCCACACAG-3′	5′-TCAGCAGAGTGAGCAGAAAGAT-3′
RUNX2	5′-TACGACCATGAGATTGGCAGTGA-3′	5′-TATAGGATCTGGGTGCAGGCTGA-3′
FSP1	5′-GGAGGCCCTGGATGTAATTGTG-3′	5′- CAACTTCATTGTCCCTGTTGCTG-3′
GPX4	5′-CCCGATATGCTGAGTGTGGTTTA-3′	5′-TTCTTGATTACTTCCTGGCTCCTG-3′
SLC7A11	5′-CCCTGGCATTTGGACGCTAC-3′	5′-CTCCAGCTGACACTCGTGCTATTTA-3′
NRF2	5′-TAGATGACCATGAGTCGCTTGC-3′	5′-GCCAAACTTGCTCCATGTCC-3′
GAPDH	5′-GCACCGTCAAGGCTGAGAAC-3′	5′-TGGTGAAGACGCCAGTGGA-3′

Alkaline Phosphatase (ALP) Staining and Alizarin Red Staining (ARS)

Following treatment with various reagents and subsequent osteogenic induction for 7 or 21 days, cells were rinsed with PBS and fixed in 4% paraformaldehyde for 20 minutes. Cells were then stained with either an alkaline phosphatase (ALP) staining solution (C3206, Beyotime) for 30 minutes or 1% alizarin red S solution (G1452, Solarbio) for 15 minutes. The staining reactions were terminated with PBS, and the cells were examined and imaged under a light microscope (CKX-41, Olympus Corp, Japan).

Cell Counting Kit-8 (CCK-8)

The optimal concentration of DEX was determined by assessing cell viability across a range of concentrations (0, 10^{-8}, 10^{-7}, 10^{-6}, and 10^{-5} mol/L). Subsequently, the optimal concentration of VK_2 was evaluated in combination with 10^{-6} mol/L DEX. The experimental concentrations of DEX and VK_2 were ultimately determined to be 10^{-6} M. To investigate the mechanism by which DEX affects osteoblast viability, cells pretreated with DEX were separately exposed to inhibitors of ferroptosis (ferrostatin-1, Fer-1 5 mM), autophagy (3-methyladenine, 3-MA 5 mM), and necroptosis (necrostatin-1, Nec-1 50μM). Cell viability was then assessed in each treatment group.

Measurement of the Intracellular ROS Level

The intracellular ROS levels in MC3T3-E1 cells were measured using both flow cytometry and DCFH-DA staining. For flow cytometry, the MC3T3-E1 cells were collected and washed with PBS after treatment with various drugs, followed by incubation with DCFH-DA (1:1000 dilution) for 20 minutes at 37 °C. ROS levels were then analyzed by flow cytometry (CytoFLEX S, Beckman) after an additional PBS wash for DCFH-DA staining, the procedures were similar except that the cells were maintained on the dish throughout the entire process, and a fluorescence microscope (OLYMPUS, FV3000) was used to capture fluorescence images.

Measurement of Mitochondrial Quantity and Mitochondrial Membrane Potential

To assess mitochondrial content, the Mito-Tracker Green kit (C1048, Beyotime Biotechnology, China) was used. After cells were subjected to various drug treatments, the culture medium was removed and replaced with pre-warmed Mito-Tracker Green staining solution, which was incubated with the cells at 37 °C for 15–45 minutes. The staining solution was then removed, and fresh pre-warmed culture medium was added. Subsequently, fluorescence images were captured using a fluorescence microscope (OLYMPUS, FV3000).

To detect mitochondrial membrane potential, cells were washed with PBS and stained with JC-1 staining solution (C1048, Beyotime Biotechnology, China), followed by incubation at 37 °C for 20 minutes. After incubation, the supernatant was aspirated, and the cells were washed twice with 1× JC-1 staining buffer. Fresh culture medium was then added, and fluorescence images were captured using a fluorescence microscope (OLYMPUS, FV3000).

Detection of Malondialdehyde (MDA)

After discarding the supernatant, cells were washed twice with PBS and harvested using a cell scraper. Total protein was extracted via lysis according to the instructions of the assay kit (S0131S, Beyotime Biotechnology, China), and the lysate was divided for subsequent protein quantification and MDA analysis. For MDA measurement samples were incubated in a ≥95°C water bath for 40 minutes, rapidly cooled under running water, and centrifuged at 4,000 rpm for 10 minutes. The absorbance of the supernatant was then measured at 530 nm using a microplate reader.

Determination of GSH Levels

The cells were washed twice with PBS, pelleted by centrifugation, and resuspended in three volumes of protein removal reagent. The samples then underwent two rapid freeze–thaw cycles using liquid nitrogen and a 37 °C water bath, followed by incubation at 4 °C for 5 minutes and centrifugation at 10,000 × g for 10 minutes. Glutathione levels were quantified using the GSH/GSSG Assay Kit (S0053, Beyotime) according to the manufacturer's protocol. Absorbance was measured at 410 nm using a microplate reader, and GSH concentrations were calculated based on a standard curve.

C11-BODIPY and FerroOrange Staining

Lipid peroxidation levels in cells were assessed using the fluorescent probe C11-BODIPY 581/591 (APExBIO, USA). Cells were seeded into culture dishes, and after removing the culture medium, they were incubated with C11-BODIPY 581/591 in serum-free medium at 37°C for 30 minutes in the dark. The intracellular Fe^{2+} levels were measured using the fluorescent probe FerroOrange (Dojindo Laboratories, China) according to the manufacturer's instructions. Following treatment, cells were washed twice with PBS and incubated with 1 μM FerroOrange diluted in serum-free medium at 37 °C for 30 minutes in the dark. Finally, the labeled cells were observed using a confocal laser scanning microscope (OLYMPUS, FV3000).

NRF2-siRNA Knockdown of Osteoblasts

The siRNA, designed and synthesized by General Biol (General Biol, China), was transfected into cells at 70–90% confluence using Lipofectamine 8000 (C0533, Beyotime) per the manufacturer's protocol. Transfection efficiency was evaluated by PCR 24 hours post-transfection.

Measurement of Reduced Coenzyme Q10 (CoQ10H2) by Enzyme-Linked Immunosorbent Assay (ELISA)

The concentration of CoQ10H2 in mouse cell was quantified using a commercial ELISA kit (CB14527-Mu, Coibo Bio, China), according to the manufacturer's instructions.

Docking Analysis

The structures of VK_2 and NRF2 were retrieved from the PubChem database, and energy minimization was performed using ChemBio3D. Based on its amino acid sequence, the NRF2 protein structure was initially modeled using AlphaFold2 and subsequently refined on the Maestro 11.9 platform to obtain the most energetically favorable docking conformation. The identification of active binding pockets, conformational space exploration, and detailed protein-ligand interaction analysis were conducted using Schrödinger Maestro, thereby enabling an efficient and comprehensive structural analysis.

Immunofluorescence (IF) Staining

The expression of NRF2 and HO-1 in MC3T3-E1 cells was assessed by IF. Following different treatments, cells were fixed with 4% paraformaldehyde for 20 minutes and then blocked with PBS containing 5% BSA for 1 hour. Subsequently, the cells were incubated overnight at 4 °C with either anti-NRF2 (1:200; T55136, Abmart) or anti-HO-1 (1:200; T55113, Abmart) primary antibodies. The next day, cells were incubated with a secondary antibody (CoraLite488-conjugated Goat Anti-Mouse, 1:200; SA00013-1, Proteintech) for 1 hour. Nuclei were stained with 4′,6-diamidino-2-phenylindole (DAPI), and fluorescence images were captured using a fluorescence microscope (OLYMPUS, FV3000).

Statistical Analysis

All data were expressed as mean ± standard deviation, based on a minimum of five independent biological replicates. Statistical analyses were performed using SPSS 25 software (SPSS. Inc., Chicago, Illinois, USA). To assess differences among three or more groups, one-way analysis of variance (ANOVA) was conducted, followed by the Least Significant Difference (LSD) tests for multiple comparisons. A $p < 0.05$ was considered statistically significant for all analyses.

Results

VK_2 Alleviated DEX-Induced Bone Loss and Enhanced Osteogenesis

Micro-CT was used to evaluate differences in bone quantity and quality among the control, DEX, and DEX+VK_2 groups. Compared with the controls, the DEX group exhibited significantly fewer and sparser trabeculae, an enlarged marrow cavity, and thinner cortical bone. In contrast, DEX+VK_2 group resulted in a marked increase in trabecular bone volume, a reduction in marrow cavity size, and restoration of cortical bone thickness (Figure 1A). HE staining in the control group revealed regularly

arranged trabeculae with greater thickness and narrower spacing. In the DEX group, the number of trabeculae was markedly reduced, with disorganized structure and increased spacing. Masson staining demonstrated a substantial decrease in bone regeneration in the DEX group, whereas bone regeneration was enhanced in the DEX+VK_2 group (Figure 1B). Following VK_2 administration, trabecular structure, density, and thickness were significantly restored, and spacing was notably reduced (Figure 1B and C). IHC staining revealed that expression levels of ALP and OCN were significantly decreased in the metaphyseal region of GIOP mice, but were significantly restored following VK_2 treatment (Figure 1D and E). Optimal concentrations of DEX and VK_2 (1×10^{-6} mol/L) were determined using cell viability assays (Figure 1F). In vitro experiments further examined the effects of DEX and VK_2 on osteogenesis in MC3T3-E1 cells. Both WB and RT-qPCR analyses showed that DEX markedly suppressed the expression of ALP, RUNX2, and OCN, whereas VK_2 treatment reversed these effects (Figure 1G and H). ALP and ARS staining further supported these findings (Figure 1I).

VK_2 Reversed the Ferroptosis Induced by DEX

The Fer-1 (inhibitor of ferroptosis) and 3MA (inhibitor of autophagy) significantly rescued the cell viability of MC3T3-E1, especially the Fer-1 (Figure 2A). This result indicated that the reduced cell viability by DEX mainly attributed to ferroptosis. The intracellular ROS levels in different groups were detected by flow cytometry and DCFH-DA staining. Both flow cytometry and DCFH-DA staining indicated that ROS level in the DEX group were significantly higher than

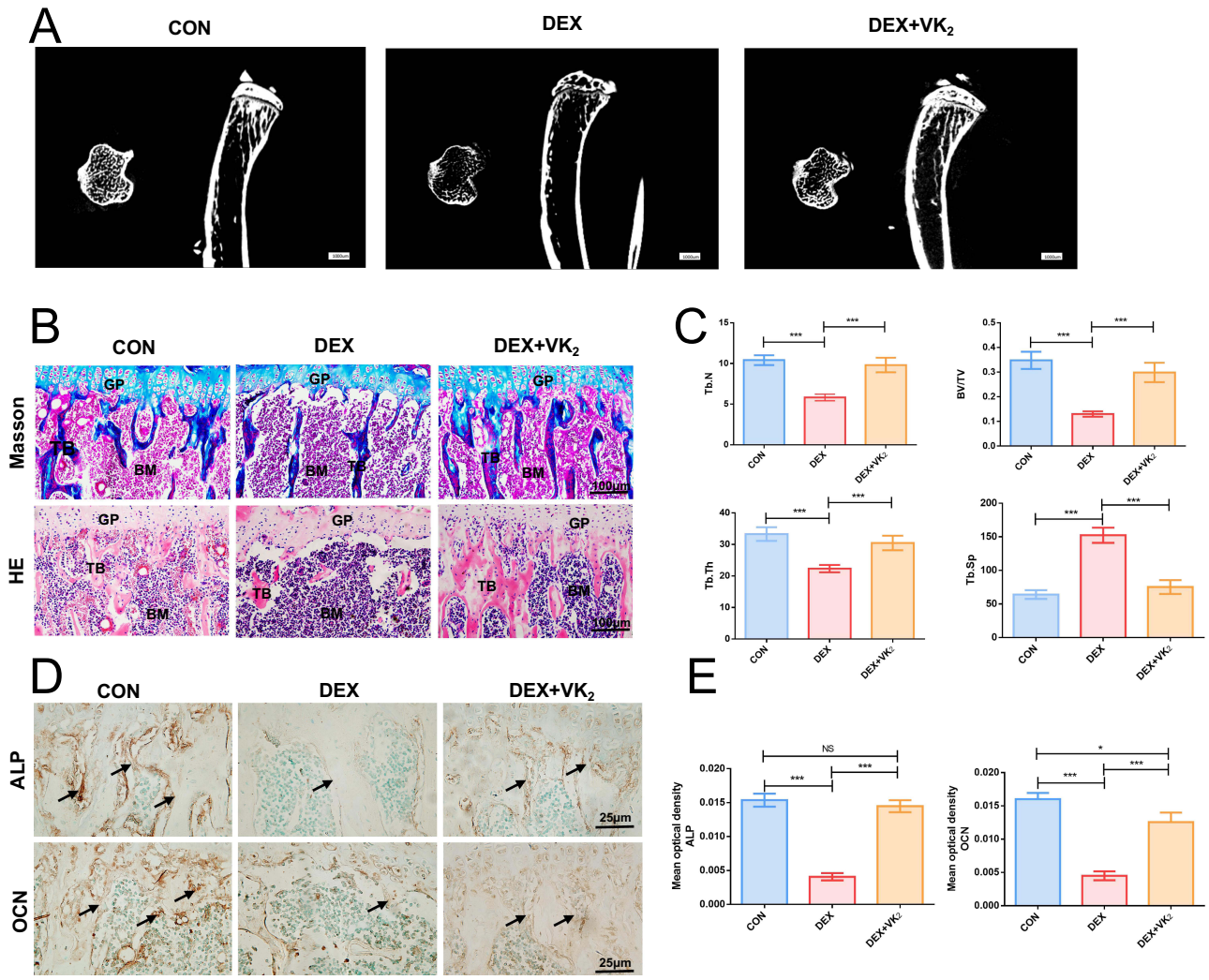

Figure 1 Continued.

https://doi.org/10.2147/DDDT.S554610

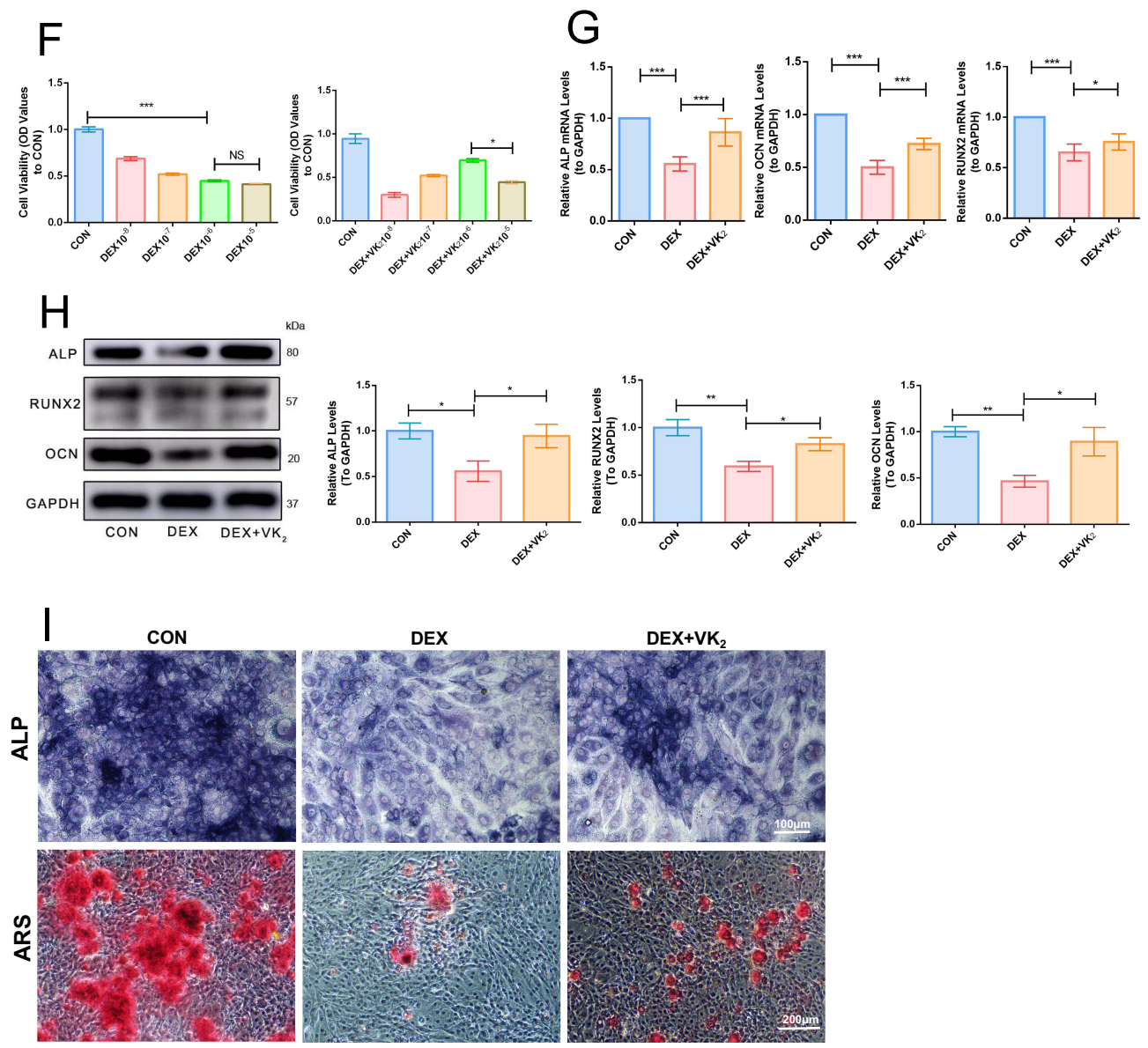

Figure 1 VK_2 alleviated DEX-induced bone loss and enhanced osteogenesis. (**A**) Representative Micro-CT images of the femur in different groups, bar=1000μm. (**B**) HE and Masson staining images of mouse femur, bar=100μm. GP, Growth Plate; TB, trabecular bone; BM, bone marrow. (**C**) Quantitative analysis of bone morphology including trabecular bone number (Tb.N), bone/tissue volume (BV/TV), trabecular bone thickness (Tb.Th) and trabecular separation (Tb.Sp), was performed in different groups using femur HE staining (n=5). (**D**) IHC staining images of mouse femur for ALP and OCN, bar=25μm. Black arrows point to the positive immunohistochemical staining regions. (**E**) Statistical analysis of IHC staining for ALP and OCN in femur of WT, DEX, and DEX+VK_2 groups (n=5). (**F**) Cell viability of MC3T3-E1 cells after treatment of different concentrations of DEX and combination of DEX and VK_2 (n=5). (**G**) The mRNA expression of ALP, OCN and RUNX2 in MC3T3-E1 cells were detected by RT-qPCR (n=5). (**H**) The protein expression of ALP, RUNX2 and OCN in MC3T3-E1 cells were detected by WB (n=5). (**I**) ALP and ARS staining of MC3T3-E1 cells in groups of control, DEX and DEX+VK_2. Data are presented as mean ± SD, n=5, $^*P < 0.05$, $^{**}P < 0.01$, $^{***}P < 0.001$.
Abbreviation: NS, no significant.

those in the control group. After VK_2 treatment the ROS level decreased in the DEX+VK_2 group. However, the ferroptosis inducer FIN56 inhibited the down-regulation effect of VK_2 on ROS (Figure 2B and C). Since ferroptosis is usually accompanied by a decrease in mitochondrial membrane potential, the corresponding detection was carried out for each group. The experimental results indicated that DEX led to a decrease in mitochondrial membrane potential, and VK_2 treatment significantly upregulated the mitochondrial membrane potential. However, the use of the ferroptosis inducer FIN56 inhibited the upregulation effect of VK_2 on mitochondrial membrane potential (Figure 2D). Mito-Tracker Green staining also indicated that DEX treatment resulted in mitochondrial damage, whereas VK_2 ameliorated the mitochondrial status, and this improvement was achieved through the inhibition of ferroptosis (Figure 2E). It is known

that GSH depletion can induce ferroptosis, and MDA is an important biomarker of ferroptosis. Therefore, the expression of the key regulatory molecules of ferroptosis, GSH and the lipid peroxidation marker MDA, were detected. The results suggested that DEX downregulated the expression of GSH and led to the upregulation of MDA, indicating that DEX induced ferroptosis. VK_2 significantly upregulated GSH and downregulated MDA, inhibiting ferroptosis. However, when the ferroptosis inducer FIN56 was used, the inhibitory effect of VK_2 on ferroptosis was significantly weakened (Figure 2F and G). Moreover, lipid peroxidation assay with BODIPY 581/591 C11 and detection of Fe^{2+} also verified that VK_2 ameliorated the ferroptosis induced by DEX (Figure 2H–K).

VK_2 Promoted Osteogenic Differentiation of Osteoblasts by Inhibiting Ferroptosis

To verify the effect of ferroptosis on the osteogenic differentiation of MC3T3-E1 cells, four groups of cells were set up, including the control group, DEX group, DEX + VK_2 group, and DEX + VK_2 + FIN56 group. The expressions of osteogenesis-related factors including ALP, RUNX2 and OCN were detected by WB and RT-qPCR, and the effect of different treatment on osteogenic differentiation of MC3T3-E1 were detected by ALP and ARS staining. Both RT-qPCR

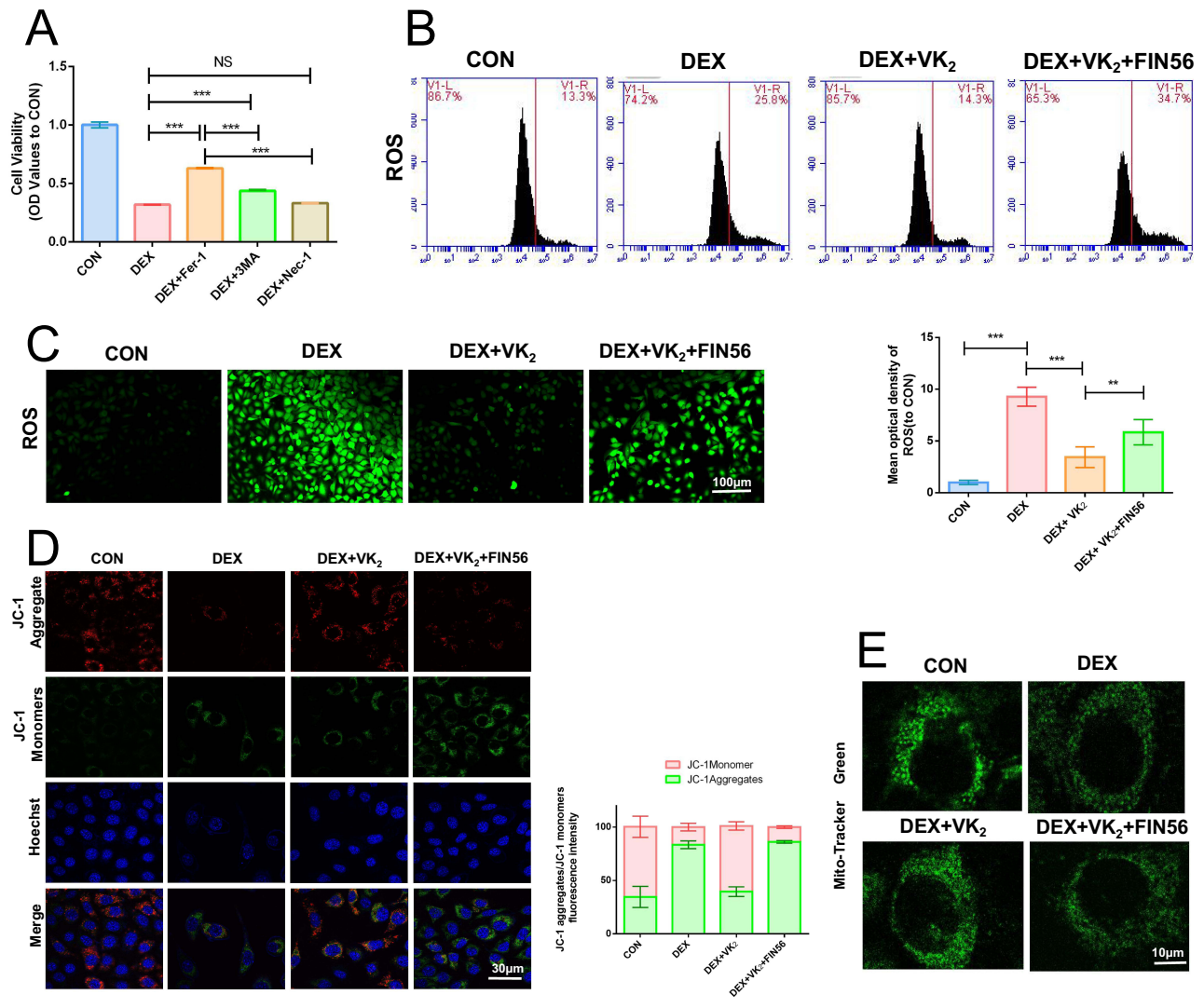

Figure 2 Continued.

https://doi.org/10.2147/DDDT.S554610

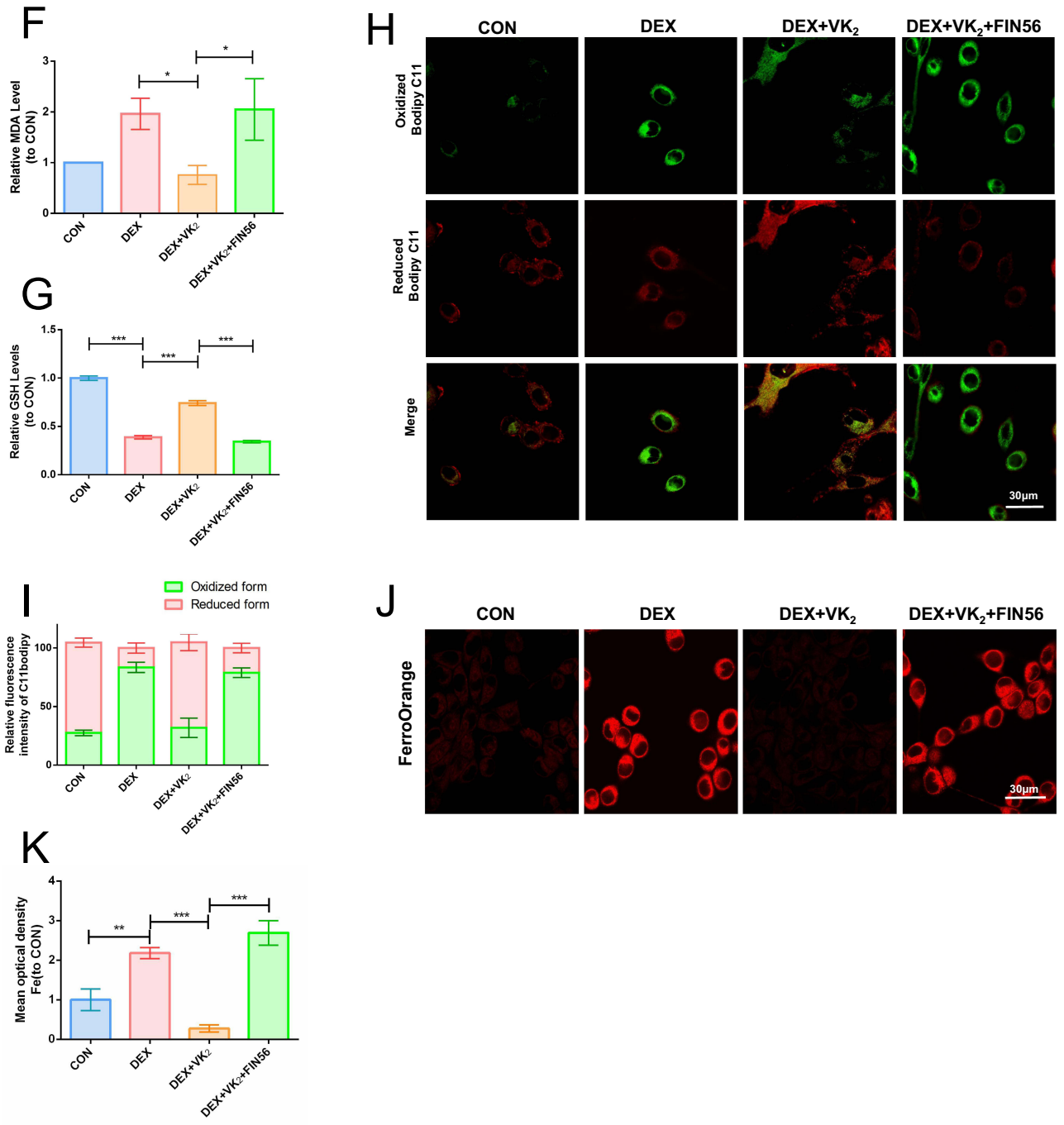

Figure 2 VK_2 reversed the ferroptosis of osteoblasts induced by DEX. (**A**) Cell viability of MC3T3-E1 cells in groups of control, DEX, DEX+Fer-1, DEX+3MA, DEX+Nec-1 (n=5). (**B**) Flow cytometric quantification of cellular ROS levels. (**C**) DCFH-DA staining detection and quantification of cellular ROS levels (n=5), bar=100μm. (**D**) JC-1 fluorescence staining for mitochondrial membrane potential and statistical analysis (n=5), bar=30μm. (**E**) Mito-Tracker Green fluorescence staining. bar=10μm. (**F**) Quantification of MDA in different groups (n=5). (**G**) Quantification of GSH in different groups (n=5). (**H**) Fluorescence staining of BODIPY 581/591 C11.bar=30μm. (**I**) Quantification of BODIPY 581/591 C11 (n=5). (**J**) Fluorescence staining of Fe^{2+}. bar=30μm. (**K**) Quantification of Fe^{2+} (n=5). Data are presented as mean ± SD, n=5, $^{*}P < 0.05$, $^{**}P < 0.01$, $^{***}P < 0.001$.

Abbreviation: NS, no significant.

(Figure 3A) and WB (Figure 3B–E) indicated that DEX inhibited the expression of these osteogenesis-related factors and VK_2 improved osteogenesis level, but the ferroptosis inducer FIN56 inhibited the osteogenesis-improving effect of VK_2. ALP and alizarin red staining also confirmed the same effect (Figure 3F and G).

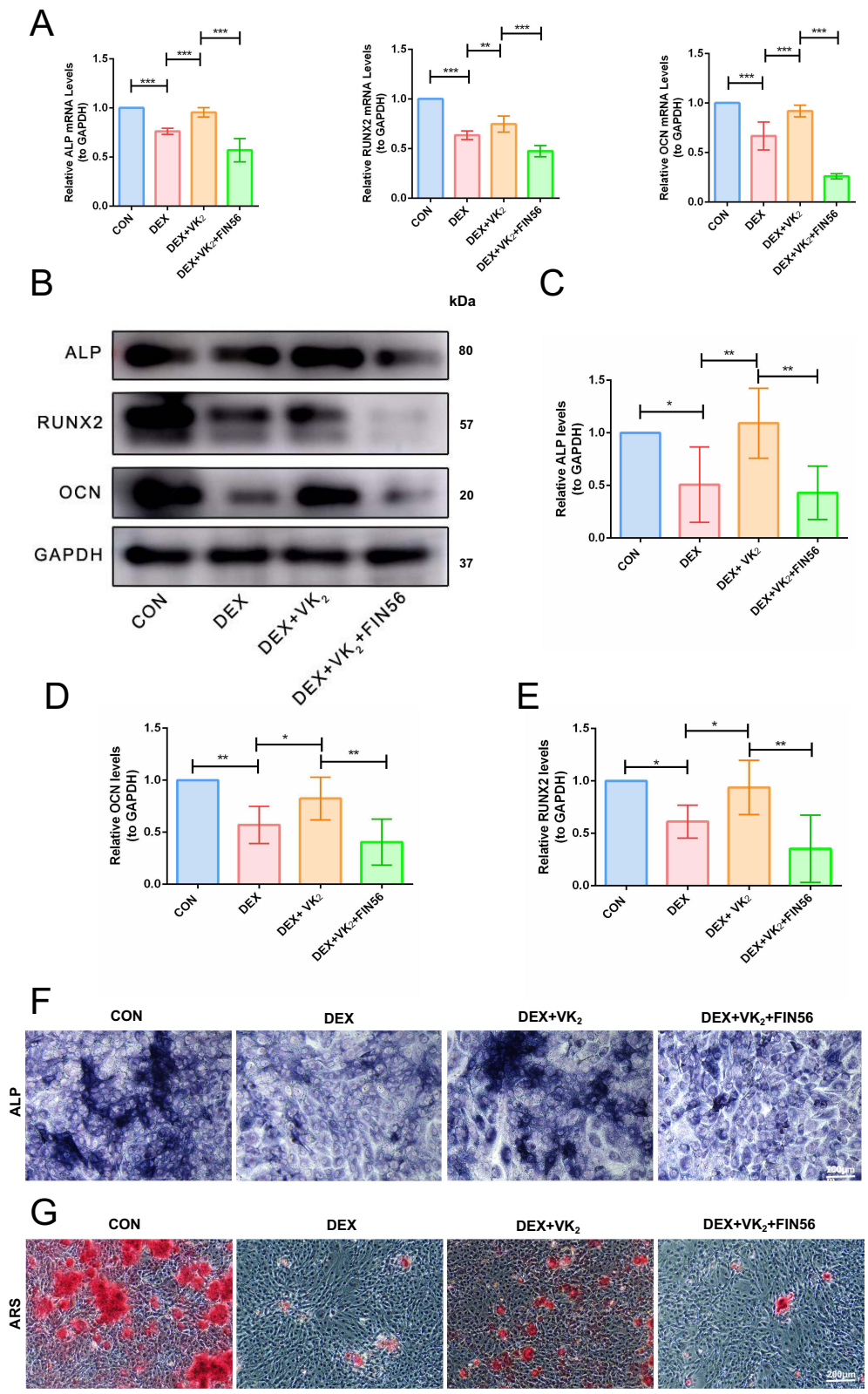

Figure 3 VK_2 promoted osteogenic differentiation of osteoblasts by inhibiting ferroptosis. (**A**) The mRNA expression of ALP, RUNX2 and OCN in MC3T3-E1 cells were detected by RT-qPCR (n=5). (**B**) The protein expression of ALP, RUNX2 and OCN in MC3T3-E1 cells were detected by WB. (**C**) Statistical analysis of the protein levels of ALP (n=5). (**D**) Statistical analysis of the protein levels of OCN (n=5). (**E**) Statistical analysis of the protein levels of RUNX2 (n=5). (**F**) ALP staining of MC3T3-E1 cells in groups of control, DEX, DEX+VK_2 and DEX+VK_2+FIN56. bar=100μm. (**G**) ARS staining of MC3T3-E1 cells in groups of control, DEX, DEX+VK_2 and DEX+VK_2+FIN56. bar=200μm. Data are expressed as mean±SD, **P*<0.05, ***P*<0.01, ****P*<0.001.

https://doi.org/10.2147/DDDT.S554610

VK_2 Promoted Osteogenic Differentiation of Osteoblasts Through Increasing FSP1

To further investigate how VK_2 regulated ferroptosis, the expressions of several significant markers of ferroptosis in MC3T3-E1 cells, including FSP1, GPX4, and SLC7A11, were detected by RT-qPCR. It was found that the expression of FSP1 was significantly downregulated by DEX and was greatly upregulated by VK_2. Moreover, the ferroptosis inducer FIN56 inhibited the up-regulatory effect of VK_2 on FSP1. In comparison with GPX4 and SLC7A11, the alterations in FSP1 were more pronounced (Figure 4A). This indicated that VK_2 predominantly regulated ferroptosis via FSP1. The protein level of FSP1 showed the same expression trend as RT-qPCR (Figure 4B). As FSP1 is closely associated with ferroptosis, the expression of FSP1 within the femurs of mice in different groups were examined and it was found that DEX significantly downregulated FSP1, while VK_2 upregulated it (Figure 4C). Rescue experiment was also performed to further verify whether VK_2 regulated ferroptosis via FSP1. Four groups of cells were established, including the control group, the DEX group, the DEX+VK_2 group, and the DEX+VK_2+iFSP1 group. Subsequently, ferroptosis-related assays were performed, including the intracellular ROS levels (Figure 4D), mitochondrial membrane potential (Figure 4E), mitochondria Mito-Tracker Green staining (Figure 4F), the expressions of MDA (Figure 4G) and lipid peroxide level (Figure 4H). All these ferroptosis-related assays suggested that VK_2 alleviated DEX-induced ferroptosis, but the use of iFSP1 significantly attenuated the inhibitory effect of VK_2 on ferroptosis. To ascertain the dominant role of the FSP1 pathway in VK_2-mediated ferroptosis inhibition, we compared the effects of the GPX4 inhibitor RSL3 and the FSP1 inhibitor iFSP1. Also, we measured changes in the levels of CoQ10H2, the product of FSP1, following treatment with DEX and VK_2 using ELISA. The results demonstrated that VK_2 significantly reversed the DEX-induced decrease in CoQ10H2 levels and iFSP1 was markedly more potent than RSL3 in inducing ferroptosis and, correspondingly, in reversing the protective effect of VK_2, which exhibited only a partial reversal (Figure 4I and J). Furthermore, RT-qPCR and WB detections were carried out to investigate the expressions of different osteogenesis-related factors, including ALP, RUNX2, and OCN. The results suggested that VK_2 improved the inhibitory effect of DEX on osteogenic factors. However, the application of the iFSP1 significantly weakened the up-regulatory effect of VK_2 on osteogenic factor (Figure 4K and L). ALP and alizarin red staining also confirmed the similar effect of DEX, VK_2 and iFSP1 (Figure 4M).

NRF2/FSP1 Was an Important Signaling Axis for VK_2 to Improve Ferroptosis

In accordance with previous research reports, NRF2 is likely to be located upstream of FSP1. Consequently, we performed molecular docking between VK_2 and NRF2. To further investigate the specific mechanism through which VK_2 inhibits ferroptosis, software of artificial intelligence was used to simulate the molecular docking between VK_2 and the NRF2 target protein. Subsequently, the docking of the complex was visualized, revealing that VK_2 formed a stable complex with NRF2 through ALA-28 and ASN-88. These simulations indicated a strong relationship between the VK_2 and NRF2 (Figure 5A). To verify this conclusion, IHC staining was performed on the femurs of the control group, DEX group, and DEX+VK_2 group of mice. It was found that compared with the control group, the expression of NRF2 and HO-1 were significantly downregulated in the DEX group, while the expression levels of NRF2 and HO-1 were restored in the DEX+VK_2 group (Figure 5B). In the in vitro experiments, the expressions of NRF2 and HO-1 in MC3T3-E1 cells of the three groups were examined via IF. The staining outcomes revealed that, in line with the results of the in vivo experiments, DEX suppressed the expressions of NRF2 in the cells, while treatment with VK_2 facilitated the restoration of these two factors (Figure 5C and D). Similar results were also found for IF of HO-1 (Figure 5E and F). To further explore the regulatory relationship between NRF2 and FSP1, in vitro experiments were designed with control group, DEX group, DEX+VK_2 group, and DEX+VK_2+ML385 group. The levels of intracellular ROS (Figure 5G and H) and lipid peroxides (Figure 5I and J) were measured in each group. Both detections revealed that VK_2 significantly suppressed ferroptosis induced by DEX, while the NRF2 inhibitor attenuated the inhibitory effect of VK_2 on ferroptosis, indicating that VK_2 regulates ferroptosis via NRF2. To rule out potential off-target effects of the inhibitors, we employed siRNA-NRF2. The results showed that NRF2 depletion led to a significant accumulation of intracellular iron and reversed the protective effect of VK_2 (Figure 5K). This genetic evidence further validated our experimental findings. The regulatory role of NRF2/HO-1 on FSP1 was further verified by RT-qPCR and WB assays. RT-qPCR of NRF2 and FSP1 also showed similar tendency (Figure 5L). Protein detections indicated that DEX significantly downregulated the

expressions of NRF2, HO-1, and FSP1. VK_2 treatment upregulated the levels of these three factors, but the use of the NRF2 inhibitor attenuated the up-regulatory effect of VK_2 on HO-1 and FSP1 (Figure 5M). Beyond the pharmacological inhibition, we also employed a genetic approach. The knockdown of NRF2 similarly reduced FSP1 protein levels, corroborating our previous findings (Figure 5N). These results implied that VK_2 regulated FSP1 via the NRF2/HO-1 axis.

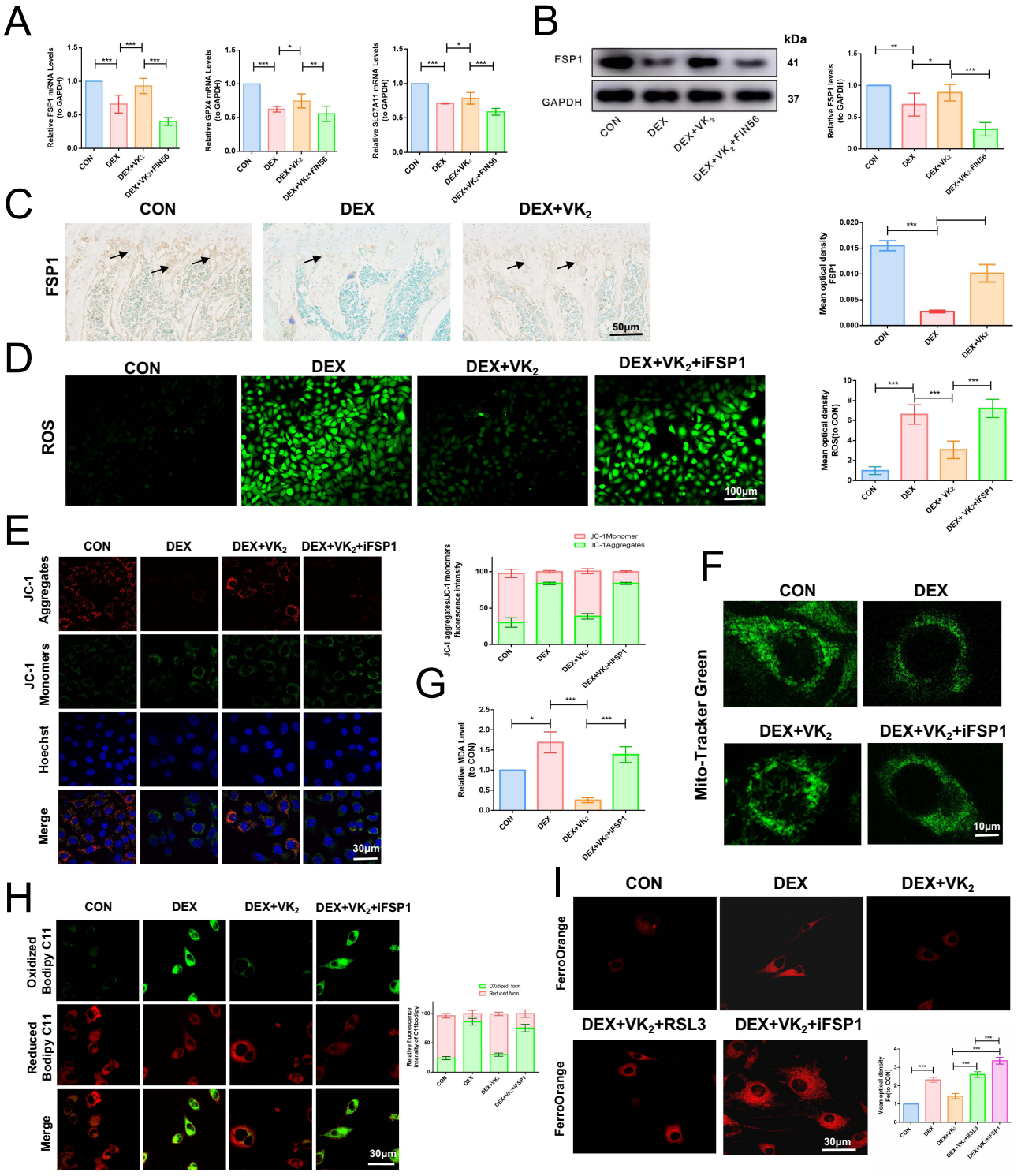

Figure 4 Continued.

https://doi.org/10.2147/DDDT.S554610

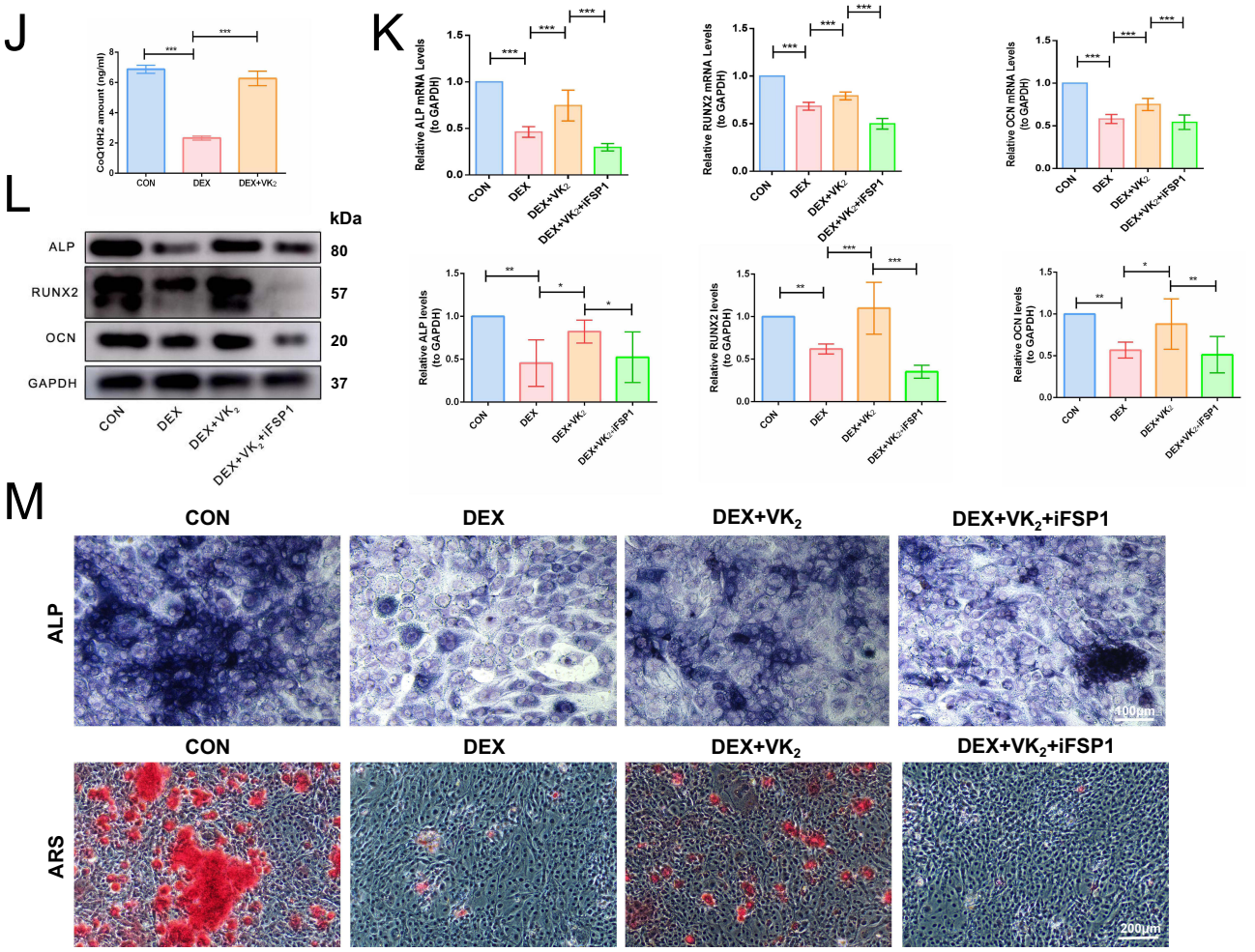

Figure 4 VK_2 promoted osteogenic differentiation of osteoblasts through increasing FSP1. (**A**) The mRNA expression of FSP1, GPX4 and SLC7A11 in MC3T3-E1 cells were detected by RT-qPCR (n=5). (**B**) The protein expression of FSP1 in MC3T3-E1 cells were detected by WB (n=5). (**C**) IHC staining and statistical analysis of FSP1 in mouse femurs (n=5), bar=50μm. Black arrows point to the positive immunohistochemical staining regions. (**D**) DCFH-DA staining detection and quantification of cellular ROS levels in MC3T3-E1 cells (n=5), bar=100μm. (**E**) JC-1 fluorescence staining for mitochondrial membrane potential and statistical analysis (n=5), bar=30μm. (**F**) Mito-Tracker Green fluorescence staining. bar=10μm. (**G**) Quantification of MDA in different groups (n=5). (**H**) Fluorescence staining and quantification of BODIPY 581/591 C11 (n=5), bar=30μm. (**I**) Fluorescence staining and quantification of Fe^{2+} (n=5), bar=30μm. (**J**) Quantification of CoQ10H2 in different groups (n=5). (**K**) The mRNA expression of ALP, RUNX2 and OCN in MC3T3-E1 cells were detected by RT-qPCR (n=5). (**L**) The protein expression of ALP, RUNX2 and OCN in MC3T3-E1 cells were detected by WB (n=5). (**M**) ALP and ARS staining of MC3T3-E1 cells in groups of control, DEX, DEX+VK_2 and DEX+VK_2+iFSP1. Data are presented as mean ± SD, n=5, $^*P < 0.05$, $^{**}P < 0.01$, $^{***}P < 0.001$.

The osteogenic differentiation levels of these four groups of cells were further examined by WB, RT-qPCR, ALP and ARS staining. Both WB and RT-qPCR suggested that VK_2 could alleviate the inhibitory effect of DEX on osteogenesis-related factors, while the NRF2 inhibitor attenuated the osteogenesis-enhancing effect of VK_2 (Figure 5O and P). ALP and ARS staining also pointed to the same conclusion (Figure 5Q).

Discussion

This study was designed to evaluate the therapeutic potential of VK_2 in GIOP. Initial in vivo and in vitro experiments demonstrated that VK_2 significantly alleviated DEX-induced osteoporosis by promoting osteogenesis. Furthermore, the protective effects of VK_2 were closely linked to its capacity to reverse DEX-induced ferroptosis in osteoblasts. Mechanistic analyses identified FSP1 as a critical regulatory factor. Subsequent rescue experiments confirmed that VK_2 inhibits ferroptosis in osteoblasts via activation of the NRF2/FSP1 signaling axis (Figure 6). Collectively, these findings offer new insights into the molecular mechanisms underlying VK_2-mediated protection in GIOP.

GIOP is a common secondary osteoporosis caused by long-term, medium to high-dose glucocorticoid use (≥3 months), with a dose- and duration-dependent prevalence.[34] The pathogenesis of GIOP is multifactorial and complex. In the early stages of the disease, GCs promote bone resorption by stimulating osteoclastogenesis and inhibiting the proliferation, differentiation, and function of osteoblasts. As the disease progresses to the established phase, the activities of both osteoblasts and osteoclasts are markedly suppressed, resulting in a state of low bone turnover.[35] Impaired bone formation is now considered the primary pathological hallmark of GIOP.[36,37] In our previous studies, we observed a reduction in osteoclast numbers in the femoral tissue of GIOP mice compared with controls, suggesting diminished bone resorption, which may be associated with later-stage disease progression.[33] Under these conditions of globally reduced bone remodeling, impaired osteogenic capacity is widely recognized as the dominant pathogenic mechanism. Therefore, the present study focused on elucidating the molecular regulation of osteogenesis under GIOP conditions.

Recent studies have revealed that the pathogenesis of GIOP is intricately associated with mitochondrial dysfunction, oxidative stress, and ferroptosis.[28] Prolonged GCs exposure disrupts mitochondrial dynamics in osteoblasts and osteocytes, resulting in a decline in mitochondrial membrane potential, reduced ATP synthesis, and excessive accumulation of

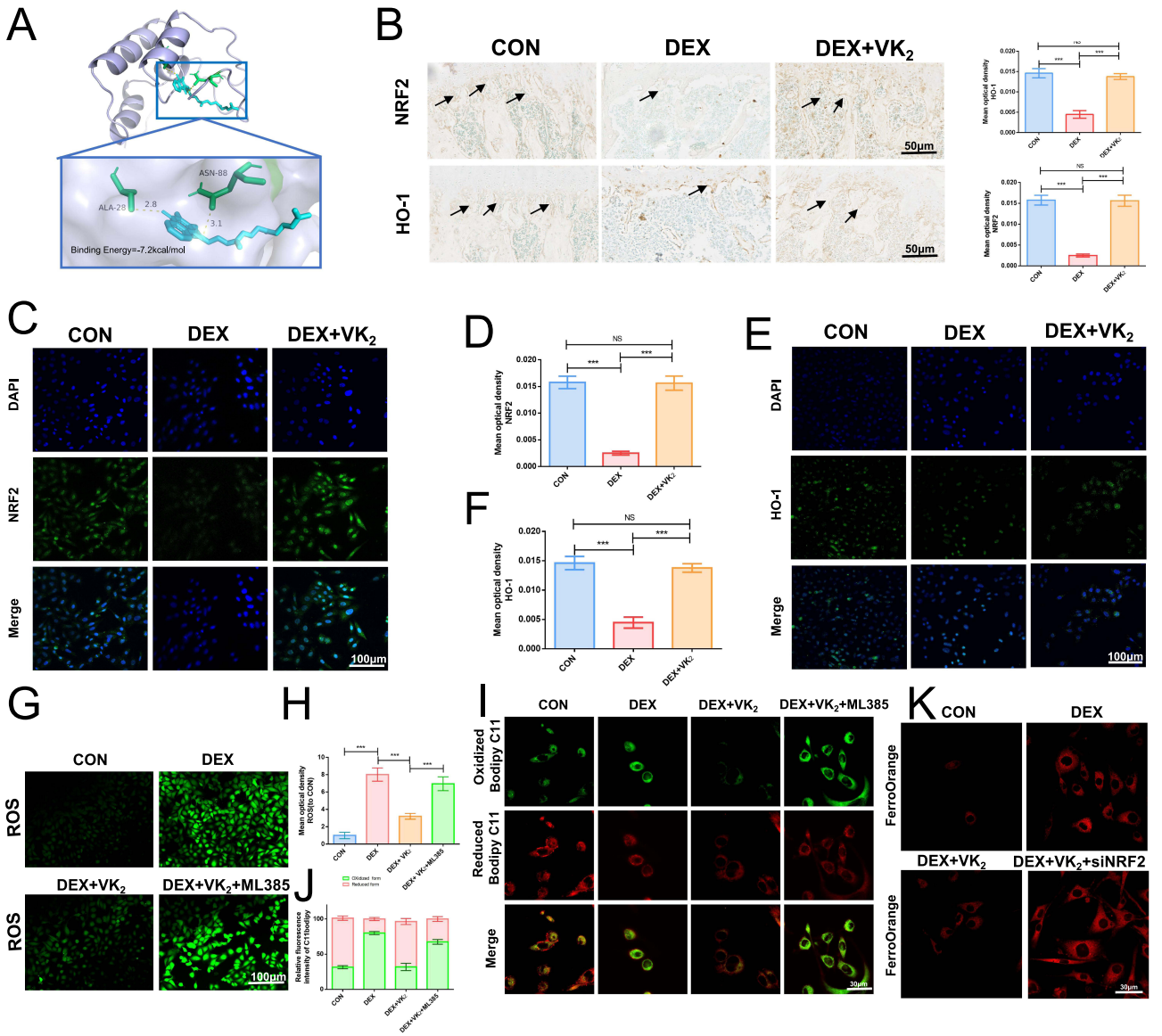

Figure 5 Continued.

https://doi.org/10.2147/DDDT.S554610

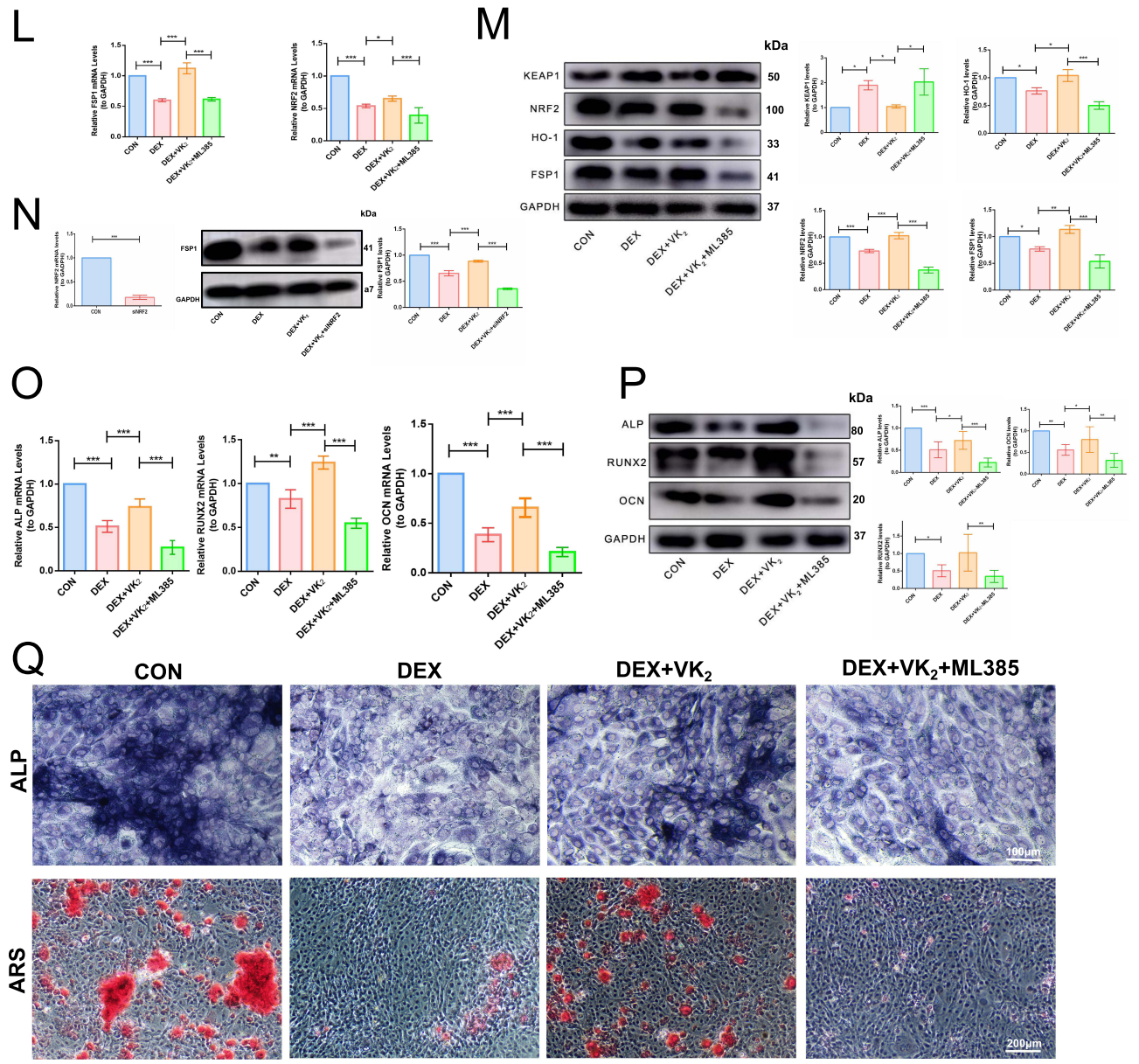

Figure 5 NRF2/FSP1 was an important signaling axis for VK_2 to improve ferroptosis. (**A**) Molecular docking analysis of VK_2 with NRF2. (**B**) IHC staining and statistical analysis of NRF2 and HO-1 in mouse femurs (n=5), bar=50μm. Black arrows point to the positive immunohistochemical staining regions. (**C**) Fluorescence staining of NRF2 in MC3T3-E1 cells. bar=100μm. (**D**) Quantification of NRF2 (n=5). (**E**) Fluorescence staining of HO-1 in MC3T3-E1 cells. bar=100μm. (**F**) Quantification of HO-1 (n=5). (**G**) DCFH-DA staining of cellular ROS levels in MC3T3-E1 cells. bar=100μm. (**H**) Quantification of cellular ROS levels (n=5). (**I**) Fluorescence staining and quantification of BODIPY 581/591 C11. bar=30μm. (**J**) Quantification of BODIPY 581/591 C11 (n=5). (**K**) Fluorescence staining of Fe^{2+} (n=5), bar=30μm. (**L**) The mRNA expression of FSP1 and NRF2 in MC3T3-E1 cells were detected by RT-qPCR (n=5). (**M**) The protein expression of KEAP1, NRF2, HO-1 and FSP1 in MC3T3-E1 cells were detected by WB (n=5). (**N**) The mRNA expression of NRF2 and protein expression of FSP1 after NRF2 knockdown by siRNA. (**O**) The mRNA expression of ALP, RUNX2 and OCN in MC3T3-E1 cells were detected by RT-qPCR (n=5). (**P**) The protein expression of ALP, RUNX2 and OCN in MC3T3-E1 cells were detected by WB (n=5). (**Q**) ALP and ARS staining of MC3T3-E1 cells in groups of control, DEX, DEX+VK_2 and DEX+VK_2+ML385. Data are presented as mean ± SD, n=5, **P* < 0.05, ***P* < 0.01, ****P* < 0.001.
Abbreviation: NS, no significant.

ROS.[38] Additionally, GCs promote lipid peroxidation by upregulating oxidase enzymes. The resulting product, MDA, further compromises membrane integrity and activates ferroptosis-related pathways.[39] Our experimental results confirmed that mitochondrial stress, lipid peroxidation, and ferroptosis were significantly elevated in both in vivo and in vitro GIOP models, highlighting the close interplay among mitochondrial dysfunction, oxidative lipid damage, and ferroptosis in the pathogenesis of GIOP.

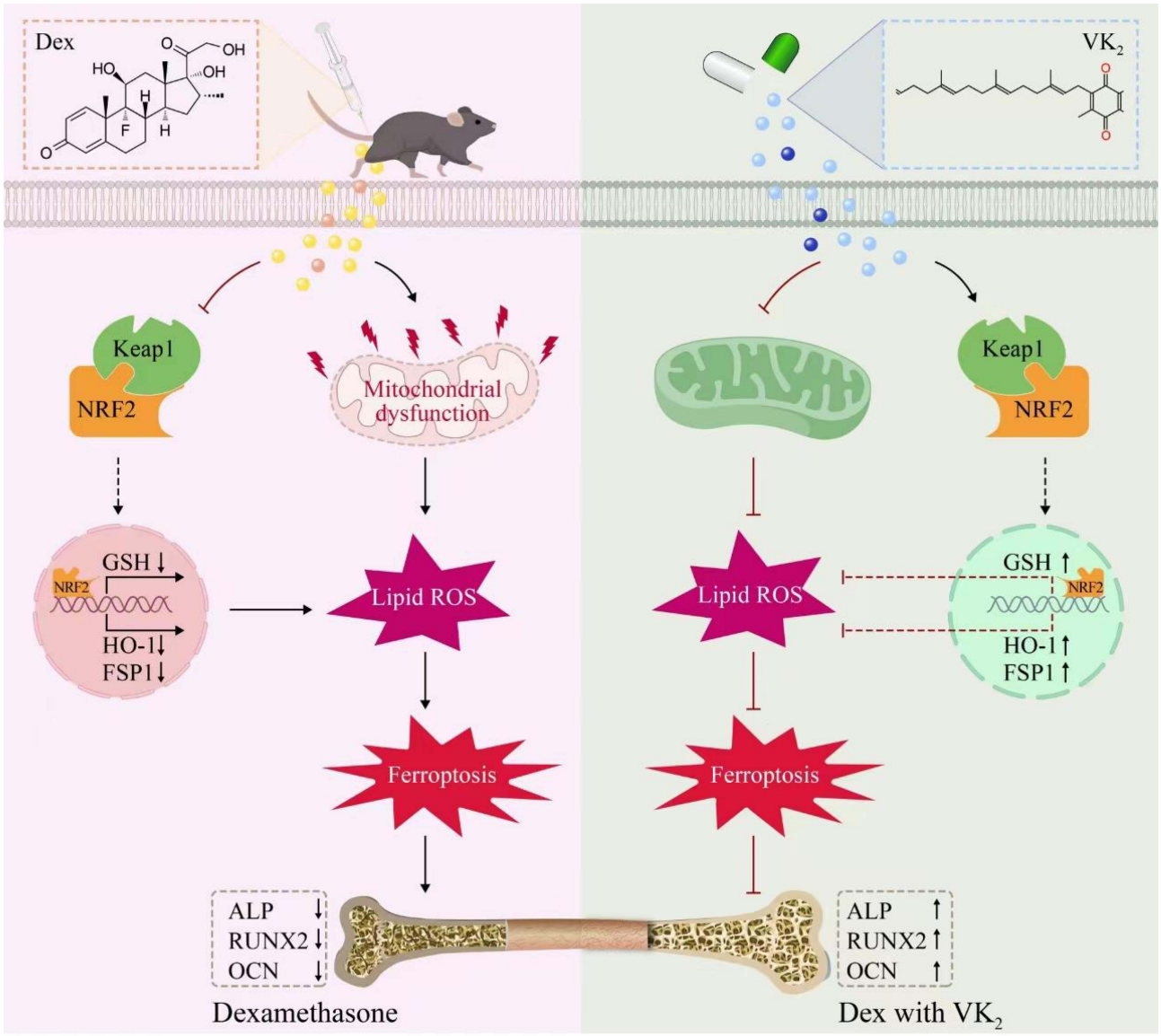

Figure 6 The mechanism of VK_2 in preventing GIOP through the NRF2/FSP1 pathway to inhibit ferroptosis in osteoblasts.

In addition to its well-documented antioxidant properties in disease modulation, VK2 promotes bone health by acting as a cofactor for γ-glutamyl carboxylase[40,41] and an SXR ligand to support mineralization and collagen accumulation,[42] as well as by suppressing the NF-κB pathway to exert dual anabolic and anti-resorptive effects.[11,43] Recent studies have also demonstrated that VK_2 inhibits osteoblast apoptosis and downregulates sclerostin expression in osteoblasts. Multiple studies have demonstrated that VK_2 exhibits significant therapeutic efficacy in ovariectomized rat models of osteoporosis.[13,43] Furthermore, VK_2 has been shown to attenuate high-glucose-induced ferroptosis in diabetic osteoporosis by reducing ROS accumulation and restoring mitochondrial function in bone marrow mesenchymal stem cells.[25] However, investigations into the preventive and therapeutic effects of VK_2 in the context of GIOP remain limited. Moreover, the relationship among VK_2, ferroptosis, and GIOP remains largely uncharacterized. In the present study, we found that DEX-induced GIOP was associated with mitochondrial stress, elevated lipid peroxidation, ferroptosis, and impaired osteogenic activity in osteoblasts. In contrast, VK_2 enhanced osteoblast differentiation and significantly improved bone mass in GIOP mice by optimizing mitochondrial function and suppressing lipid peroxidation and ferroptosis.

Ferroptosis is an iron-dependent form of programmed cell death, characterized by excessive intracellular lipid peroxidation and compromised antioxidant defense mechanisms.[39] Recent studies have shown that osteoblast ferroptosis

https://doi.org/10.2147/DDDT.S554610

plays a critical role in the pathogenesis of diabetic osteoporosis.[44,45] Similarly, GCs have been reported to induce ferroptosis in osteoblasts.[20,46] Based on current research, the role of ferroptosis in GIOP is not a ubiquitous form of cell death but exhibits considerable specificity. First, a central toxicity of GCs lies in inducing mitochondrial dysfunction and severe oxidative stress, while significantly depleting intracellular essential antioxidants.[47,48] This upstream event precisely triggers the core process of ferroptosis—the uncontrolled accumulation of lipid peroxidation. Therefore, ferroptosis can be regarded as a key and specific "downstream executor" of GC-induced osteotoxicity. Second, its specificity may be highlighted in comparison with other types of osteoporosis. For instance, in postmenopausal osteoporosis, enhanced bone resorption due to estrogen deficiency is the primary characteristic, whereas in GIOP, GCs directly target and damage osteoblasts and osteocytes.[33,35] Our study observed markedly elevated key indicators of ferroptosis (such as lipid ROS and iron accumulation) in the GIOP model, and ferroptosis-specific inhibitors demonstrated potent bone-protective effects. These findings strongly suggest that ferroptosis constitutes a more distinctive pathological feature in GIOP. Finally, compared with other forms of cell death, ferroptosis appears to play a more dominant role. In this study, ferroptosis inhibitors provided significantly superior protection to osteocytes compared to autophagy or necrosis inhibitors. Collectively, this evidence indicates that ferroptosis plays a relatively specific and central role in GC-induced osteocyte death.

As a central transcription factor in the antioxidant defense system, NRF2 has been implicated in the pathogenesis of GIOP.[29,30] Previous studies indicate that VK_2 enhances the antioxidant defense capacity of endothelial cells via NRF2 activation,[49] a finding that aligns with our current results. It is important to note that the precise mechanism by which VK_2 activates NRF2—whether through direct binding or indirect upstream signaling—remains a subject for further investigation. Our molecular docking results, consistent with the findings of Lin et al, support the plausibility of a direct interaction between VK_2 and the NRF2 protein, which could underpin its anti-ferroptotic effect.[50] However, the activation of NRF2 is a complex process known to be regulated by multiple upstream pathways, including PI3K/AKT, PKC, and PERK signaling.[51–53] To our knowledge, whether VK_2 utilizes these canonical pathways to modulate NRF2 activity has not yet been experimentally demonstrated. Therefore, elucidating the exact contribution of direct binding versus alternative signaling routes represents a critical and necessary direction for future research to fully delineate VK_2's mechanism of action. Additionally, FSP1 has been identified as a GPX4-independent ferroptosis regulator, functioning through a CoQ10-dependent antioxidant system, and is emerging as a potential therapeutic target in neuroinflammation.[54] In our study, we assessed the expression of key ferroptosis-associated regulators—FSP1, GPX4, and SLC7A11—in osteoblasts under different treatment conditions. Among these, FSP1 exhibited the most pronounced recovery following VK_2 administration, suggesting that VK_2 may alleviate ferroptosis predominantly via FSP1. Immunohistochemical analysis further confirmed the differential expression of FSP1 in vivo. To validate these findings, we conducted in vitro rescue experiments using an FSP1 inhibitor, which further confirmed the role of FSP1 in VK_2-mediated osteoprotective effects. Moreover, targeted rescue assays also demonstrated that NRF2 regulates FSP1 expression. Collectively, these findings indicate that the NRF2/FSP1 signaling axis represents a promising therapeutic target for the prevention and treatment of GIOP.

The therapeutic potential of VK_2 for bone health is increasingly recognized. Clinical evidence demonstrates that VK_2 supplementation preserves or improves lumbar bone mineral density and promotes osteocalcin carboxylation, aligning with our results.[14,15] VK_2 exhibits a favorable safety profile with no significant increase in adverse events, though caution remains necessary for patients using warfarin.[55] Mechanistically, while ferroptosis inhibition has been implicated, emerging evidence suggests the involvement of other pathways including autophagy and apoptosis. Studies confirm that VK_2 promotes autophagic activation through accelerated LC3-I to LC3-II conversion, an increased LC3-II/LC3-I ratio, and upregulated Beclin-1 expression.[56,57] Future investigations should focus on delineating the contributions of these parallel pathways and validating VK_2's efficacy through well-designed clinical trials. From a pathophysiological standpoint, GIOP represents a low bone turnover state primarily driven by impaired bone formation – a context in which anabolic agents like VK_2 are theoretically advantageous. Nevertheless, the absence of large-scale randomized controlled trials specifically targeting GIOP patients continues to limit its clinical adoption, and its long-term benefits and definitive therapeutic role require further confirmation.

However, several limitations restricted the use of FIN56 in in vivo experiments. These include its high cost, unverified long-term safety in animal models, and the lack of sufficient supporting literature for in vivo applications. Therefore, a rescue experiment was not included in the in vivo component of this study. Also, despite its favorable tolerance profile, the safety of VK_2 warrants further confirmation, considering reported side effects like taste changes, potential hepatobiliary effects, and its established antagonism with warfarin. Furthermore, this study was limited to the MC3T3-E1 cell line and an animal model with an intervention period of up to 8 weeks. The effects of VK_2 on other bone cell types (eg, osteocytes) and in longer-term models warrant further investigation.

Conclusion

In conclusion, our study establishes that VK_2 can prevents GIOP by targeting a novel pathogenic mechanism—ferroptosis, thereby identifying the inhibition of ferroptosis as the primary mechanism underlying VK_2's protective effects. This finding not only provides a fresh perspective on the etiology of GIOP but also positions ferroptosis inhibition as a promising and innovative therapeutic strategy for this condition, with VK_2 emerging as a potential candidate for clinical translation. However, it is important to acknowledge the limitations of this study, including its focus on a single cell line and the absence of long-term in vivo data. Future research involving animal models and ultimately human clinical trials will be essential to validate these findings, determine the long-term efficacy and safety of VK_2, and fully establish its therapeutic potential for managing GIOP in patients.

Ethical Approval

All the animal procedures in this study were performed in accordance with the Guidelines for Care and Use of Laboratory Animals of the National Institutes of Health. All animal experiments were approved by the Institutional Animal Care and Use Committee of the Hospital of Stomatology, Shandong University (No.20230803).

Author Contributions

All authors made a significant contribution to the work reported, whether that is in the conception, study design, execution, acquisition of data, analysis and interpretation, or in all these areas; took part in drafting, revising or critically reviewing the article; gave final approval of the version to be published; have agreed on the journal to which the article has been submitted; and agree to be accountable for all aspects of the work.

Funding

This study was partially supported by the National Natural Science Foundation of China (No. 82370999) to Guo J and the Natural Science Foundation of Shandong Province (No. ZR2024QH617) to Kou Y.

Disclosure

The authors declare that they have no conflicts of interest with the contents of this article.

References

1. Vandewalle J, Luypaert A, De Bosscher K, et al. Therapeutic mechanisms of glucocorticoids. *Trends Endocrinol Metab*. 2018;29(1):42–54. doi:10.1016/j.tem.2017.10.010
2. Chotiyarnwong P, McCloskey EV. Pathogenesis of glucocorticoid-induced osteoporosis and options for treatment. *Nat Rev Endocrinol*. 2020;16(8):437–447. doi:10.1038/s41574-020-0341-0
3. Pofi R, Caratti G, Ray DW, et al. Treating the side effects of exogenous glucocorticoids; can we separate the good from the bad? *Endocr Rev*. 2023;44(6):975–1011. doi:10.1210/endrev/bnad016
4. Adami G, Saag KG. Glucocorticoid-induced osteoporosis update. *Curr Opin Rheumatol*. 2019;31(4):388–393. doi:10.1097/bor.0000000000000608
5. Cho SK, Sung YK. Update on glucocorticoid induced osteoporosis. *Endocrinol Metab*. 2021;36(3):536–543. doi:10.3803/EnM.2021.1021
6. Buckley L, Humphrey MB. Glucocorticoid-induced osteoporosis. *N Engl J Med*. 2018;379(26):2547–2556. doi:10.1056/NEJMcp1800214
7. Chen M, Fu W, Xu H, et al. Pathogenic mechanisms of glucocorticoid-induced osteoporosis. *Cytokine Growth Factor Rev*. 2023;70:54–66. doi:10.1016/j.cytogfr.2023.03.002
8. Ivanova D, Zhelev Z, Getsov P, et al. Vitamin K: redox-modulation, prevention of mitochondrial dysfunction and anticancer effect. *Redox Biol*. 2018;16:352–358. doi:10.1016/j.redox.2018.03.013

9. He Q, Lin Y, Chen B, et al. Vitamin K2 ameliorates osteoarthritis by suppressing ferroptosis and extracellular matrix degradation through activation GPX4's dual functions. *Biomed Pharmacother*. 2024;175:116697. doi:10.1016/j.biopha.2024.116697
10. Zhang T, O'Connor C, Sheridan H, et al. Vitamin K2 in health and disease: a clinical perspective. *Foods*. 2024;13(11). doi:10.3390/foods13111646
11. Yamaguchi M, Weitzmann MN. Vitamin K2 stimulates osteoblastogenesis and suppresses osteoclastogenesis by suppressing NF-κB activation. *Int J Mol Med*. 2011;27(1):3–14. doi:10.3892/ijmm.2010.562
12. Ding F, Zhang W, Liu T, et al. MK-4 ameliorates diabetic osteoporosis in angiogenesis-dependent bone formation by promoting mitophagy in endothelial cells. *Drug Des Devel Ther*. 2025;19:2173–2188. doi:10.2147/dddt.S503930
13. Wang H, Zhang N, Li L, et al. Menaquinone 4 reduces bone loss in ovariectomized mice through dual regulation of bone remodeling. *Nutrients*. 2021;13(8). doi:10.3390/nu13082570
14. Knapen MH, Schurgers LJ, Vermeer C. Vitamin K2 supplementation improves hip bone geometry and bone strength indices in postmenopausal women. *Osteoporos Int*. 2007;18(7):963–972. doi:10.1007/s00198-007-0337-9
15. Koitaya N, Sekiguchi M, Tousen Y, et al. Low-dose vitamin K2 (MK-4) supplementation for 12 months improves bone metabolism and prevents forearm bone loss in postmenopausal Japanese women. *J Bone Miner Metab*. 2014;32(2):142–150. doi:10.1007/s00774-013-0472-7
16. Cheung AM, Tile L, Lee Y, et al. Vitamin K supplementation in postmenopausal women with osteopenia (ECKO trial): a randomized controlled trial. *PLoS Med*. 2008;5(10):e196. doi:10.1371/journal.pmed.0050196
17. Shiraki M, Shiraki Y, Aoki C, et al. Vitamin K2 (menatetrenone) effectively prevents fractures and sustains lumbar bone mineral density in osteoporosis. *J Bone Miner Res*. 2000;15(3):515–521. doi:10.1359/jbmr.2000.15.3.515
18. Cockayne S, Adamson J, Lanham-New S, et al. Vitamin K and the prevention of fractures: systematic review and meta-analysis of randomized controlled trials. *Arch Intern Med*. 2006;166(12):1256–1261. doi:10.1001/archinte.166.12.1256
19. Cui Y, Zhang W, Yang P, et al. Menaquinone-4 prevents medication-related osteonecrosis of the jaw through the SIRT1 signaling-mediated inhibition of cellular metabolic stresses-induced osteoblast apoptosis. *Free Radic Biol Med*. 2023;206:33–49. doi:10.1016/j.freeradbiomed.2023.06.022
20. Jiang Y, Ye AH, He WG, et al. Reducing PDK4 level constitutes a pivotal mechanism for glucocorticoids to impede osteoblastic differentiation through the enhancement of ferroptosis in mesenchymal stem cells. *Stem Cell Res Ther*. 2025;16(1):91. doi:10.1186/s13287-025-04186-9
21. Zheng H, Lin H, Ke Y, et al. Piezoelectric-triggered ferroptosis for cancer therapy via cascade-enhanced immune response. *Adv Healthc Mater*. 2025:e2501339. doi:10.1002/adhm.202501339
22. Dong W, Xiao Z, Ma H, et al. A mitochondrial targeted near-infrared ratio fluorescent probe for ferroptosis related hydrogen polysulfides imaging in arthritis. *J Colloid Interface Sci*. 2025;695:137774. doi:10.1016/j.jcis.2025.137774
23. Doll S, Freitas FP, Shah R, et al. FSP1 is a glutathione-independent ferroptosis suppressor. *Nature*. 2019;575(7784):693–698. doi:10.1038/s41586-019-1707-0
24. Bersuker K, Hendricks JM, Li Z, et al. The CoQ oxidoreductase FSP1 acts parallel to GPX4 to inhibit ferroptosis. *Nature*. 2019;575(7784):688–692. doi:10.1038/s41586-019-1705-2
25. Jin C, Tan K, Yao Z, et al. A novel anti-osteoporosis mechanism of VK2: interfering with ferroptosis via AMPK/SIRT1 pathway in type 2 diabetic osteoporosis. *J Agric Food Chem*. 2023;71(6):2745–2761. doi:10.1021/acs.jafc.2c05632
26. Zhang Z, Ji C, Wang YN, et al. Maresin1 suppresses high-glucose-induced ferroptosis in osteoblasts via NRF2 activation in type 2 diabetic osteoporosis. *Cells*. 2022;11(16). doi:10.3390/cells11162560
27. Yang Y, Lin Y, Wang M, et al. Targeting ferroptosis suppresses osteocyte glucolipotoxicity and alleviates diabetic osteoporosis. *Bone Res*. 2022;10(1):26. doi:10.1038/s41413-022-00198-w
28. Khatun J, Gelles JD, Chipuk JE. Dynamic death decisions: how mitochondrial dynamics shape cellular commitment to apoptosis and ferroptosis. *Dev Cell*. 2024;59(19):2549–2565. doi:10.1016/j.devcel.2024.09.004
29. Luo T, Song S, Wang S, et al. Mechanistic insights into cadmium-induced nephrotoxicity: NRF2-Driven HO-1 activation promotes ferroptosis via iron overload and oxidative stress in vitro. *Free Radic Biol Med*. 2025;235:162–175. doi:10.1016/j.freeradbiomed.2025.04.047
30. Cheng X, Hao W, Yu S, et al. Nephroprotective effects of Amomum kravanh essential oil by inhibition of ferroptosis regulated by Nrf2/HO-1 signaling pathway. *Phytomedicine*. 2025;142:156762. doi:10.1016/j.phymed.2025.156762
31. Li G, Liu R, Peng Z, et al. Inhibition of CAV1 attenuates diabetic cardiomyopathy through reducing ferroptosis via activating NRF2/GCLC signaling pathway. *Theranostics*. 2025;15(11):4989–5006. doi:10.7150/thno.107367
32. Koppula P, Lei G, Zhang Y, et al. A targetable CoQ-FSP1 axis drives ferroptosis- and radiation-resistance in KEAP1 inactive lung cancers. *Nat Commun*. 2022;13(1):2206. doi:10.1038/s41467-022-29905-1
33. Rong X, Kou Y, Zhang Y, et al. ED-71 prevents glucocorticoid-induced osteoporosis by regulating osteoblast differentiation via notch and Wnt/β-Catenin pathways. *Drug Des Devel Ther*. 2022;16:3929–3946. doi:10.2147/dddt.S377001
34. Humphrey MB, Russell L, Danila MI, et al. 2022 American College of rheumatology guideline for the prevention and treatment of glucocorticoid-induced osteoporosis. *Arthritis Rheumatol*. 2023;75(12):2088–2102. doi:10.1002/art.42646
35. Kobza AO, Herman D, Papaioannou A, et al. Understanding and managing corticosteroid-induced osteoporosis. *Open Access Rheumatol*. 2021;13:177–190. doi:10.2147/oarrr.S282606
36. Han Y, Zhang L, Xing Y, et al. Autophagy relieves the function inhibition and apoptosis-promoting effects on osteoblast induced by glucocorticoid. *Int J Mol Med*. 2018;41(2):800–808. doi:10.3892/ijmm.2017.3270
37. Gado M, Baschant U, Hofbauer LC, et al. Bad to the bone: the effects of therapeutic glucocorticoids on osteoblasts and osteocytes. *Front Endocrinol*. 2022;13:835720. doi:10.3389/fendo.2022.835720
38. Lin YZ, Chen ZH, Yang JF, et al. Astaxanthin prevents glucocorticoid-induced femoral head osteonecrosis by targeting ferroptosis through the JAK2/STAT3 signaling pathway. *J Agric Food Chem*. 2025;73(7):4270–4287. doi:10.1021/acs.jafc.4c09284
39. Noguchi N, Saito Y, Niki E. Lipid peroxidation, ferroptosis and antioxidants. *Free Radic Biol Med*. 2025. doi:10.1016/j.freeradbiomed.2025.05.393
40. Wang R, Chen B, Elghobashi-Meinhardt N, et al. Structure and mechanism of vitamin-K-dependent γ-glutamyl carboxylase. *Nature*. 2025;639(8055):808–815. doi:10.1038/s41586-024-08484-9
41. Shearer MJ, Okano T. Key pathways and regulators of vitamin K function and intermediary metabolism. *Annu Rev Nutr*. 2018;38:127–151. doi:10.1146/annurev-nutr-082117-051741
42. Suhara Y, Hanada N, Okitsu T, et al. Structure-activity relationship of novel menaquinone-4 analogues: modification of the side chain affects their biological activities. *J Med Chem*. 2012;55(4):1553–1558. doi:10.1021/jm2013166

43. Lee AS, Sung MJ, Son SJ, et al. Effect of menaquinone-4 on receptor activator of nuclear factor κB ligand-induced osteoclast differentiation and ovariectomy-induced bone loss. *J Med Food*. 2023;26(2):128–134. doi:10.1089/jmf.2022.K.0078
44. Wei F, Ruan B, Dong J, et al. Asperosaponin VI inhibition of DNMT alleviates GPX4 suppression-mediated osteoblast ferroptosis and diabetic osteoporosis. *J Adv Res*. 2024. doi:10.1016/j.jare.2024.11.036
45. Peng B, Feng Z, Yang A, et al. TIMP1 regulates ferroptosis in osteoblasts by inhibiting TFRC ubiquitination: an in vitro and in vivo study. *Mol Med*. 2024;30(1):226. doi:10.1186/s10020-024-01000-9
46. Zheng X, Ye FC, Sun T, et al. Delay the progression of glucocorticoid-induced osteoporosis: fraxin targets ferroptosis via the Nrf2/GPX4 pathway. *Phytother Res*. 2024;38(11):5203–5224. doi:10.1002/ptr.8310
47. Du F, Yu Q, Swerdlow RH, et al. Glucocorticoid-driven mitochondrial damage stimulates Tau pathology. *Brain*. 2023;146(10):4378–4394. doi:10.1093/brain/awad127
48. Bjelakovic G, Beninati S, Pavlovic D, et al. Glucocorticoids and oxidative stress. *J Basic Clin Physiol Pharmacol*. 2007;18(2):115–127. doi:10.1515/jbcpp.2007.18.2.115
49. El-Sherbiny M, Atef H, Helal GM, et al. Vitamin K2 (MK-7) intercepts keap-1/Nrf-2/HO-1 pathway and hinders inflammatory/apoptotic signaling and liver aging in naturally aging rat. *Antioxidants*. 2022;11(11). doi:10.3390/antiox11112150
50. Tao L, Li H, Wang J, et al. Vitamin K2 inhibits PGE2-mediated osteoblast ferroptosis by upregulation of CBR1 via the Nrf2/Keap1 pathway. *Commun Biol*. 2025;8(1):1116. doi:10.1038/s42003-025-08564-0
51. Wang B, Jin Y, Liu J, et al. EP1 activation inhibits doxorubicin-cardiomyocyte ferroptosis via Nrf2. *Redox Biol*. 2023;65:102825. doi:10.1016/j.redox.2023.102825
52. Wen X, Tang S, Wan F, et al. The PI3K/Akt-Nrf2 signaling pathway and mitophagy synergistically mediate hydroxytyrosol to alleviate intestinal oxidative damage. *Int J Biol Sci*. 2024;20(11):4258–4276. doi:10.7150/ijbs.97263
53. Wei R, Zhao Y, Wang J, et al. Tagitinin C induces ferroptosis through PERK-Nrf2-HO-1 signaling pathway in colorectal cancer cells. *Int J Biol Sci*. 2021;17(11):2703–2717. doi:10.7150/ijbs.59404
54. Chen J, Shi Z, Chen Y, et al. A CoQ10 analog ameliorates cognitive impairment and early brain injury after subarachnoid hemorrhage by regulating ferroptosis and neuroinflammation. *Redox Biol*. 2025;84:103684. doi:10.1016/j.redox.2025.103684
55. Tamadon-Nejad S, Ouliass B, Rochford J, et al. Vitamin K deficiency induced by warfarin is associated with cognitive and behavioral perturbations, and alterations in brain sphingolipids in rats. *Front Aging Neurosci*. 2018;10:213. doi:10.3389/fnagi.2018.00213
56. Yokoyama T, Miyazawa K, Naito M, et al. Vitamin K2 induces autophagy and apoptosis simultaneously in leukemia cells. *Autophagy*. 2008;4(5):629–640. doi:10.4161/auto.5941
57. Chen L, Shi X, Weng SJ, et al. Vitamin K2 can rescue the dexamethasone-induced downregulation of osteoblast autophagy and mitophagy thereby restoring osteoblast function in vitro and in vivo. *Front Pharmacol*. 2020;11:1209. doi:10.3389/fphar.2020.01209